Spectrochimica Acta Part B: Atomic Spectroscopy 193 (2022) 106437

Contents lists available at ScienceDirect

Spectrochimica Acta Part B: Atomic Spectroscopy

journal homepage: www.elsevier.com/locate/sab

Gas temperature and air fraction diagnosis of helium cold atmospheric plasmas by means of atomic emission lines

M.C. García [a,*], C. Yubero [b], A. Rodero [b]

[a] Department of Applied Physics, University of Cordoba, Campus de Rabanales, Córdoba 14071, Spain
[b] Department of Physics, University of Cordoba, Campus de Rabanales, Córdoba 14071, Spain

ARTICLE INFO

Keywords:
Plasma diagnosis
Emission spectroscopy
Gas temperature
Atmospheric pressure plasma
Cold atmospheric plasma

ABSTRACT

In this work, we present a new method allowing the determination of both the gas temperature and the air fraction in non-thermal atmospheric helium plasmas. This new UV-Atomic Emission Spectroscopy technique based on the measurement of the collisional broadening of the He I 667.82 nm and He I 728.13 nm emission lines is a particularly sensible method under low gas temperature conditions; hence it is particularly suitable for the diagnosis of cold helium atmospheric plasmas of biomedical use. To quantify the unknown amount of air entering these plasma jets is key to understanding the chemistry in them and the basis of their clinical and biological action, as it determines the amount of reactive oxygen and nitrogen they generate. The method has been applied to diagnose microwave helium plasmas generated inside three different reactors, thus in environments with different air contents.

1. Introduction

In recent years, there has been a great interest in exploring the use of non-thermal plasmas in fields such as medicine, agriculture, or food [1–3]. This has led to the development of very diverse and numerous sources of cold atmospheric plasma (CAP), with temperatures sometimes even below 40 °C, which are currently enabling previously unimaginable plasma applications. These include wound healing, treatment of cancerous lesions, plant diseases, treatment of seeds (for disinfestation, disinfection, or modification of their surface properties to improve germination and crop yield), food treatment for better conservation or avoid foodborne outbreaks, to mention just a few.

In the field of medicine, there has been a growing interest in the study of the direct application of plasmas on the human body [2,4–8]. It has been already a while since a new path in electrosurgery came up with the development of plasma-based devices. Thereby, nowadays, argon plasma coagulation (APC) and coblation are well-established electrosurgical methods relying on plasma technology [9–13]. In the same way, the PlasmaJet® device is also currently used in surgical practice to cut or coagulate tissues in a well-defined and localized manner [14]. In all these cutting and coagulation electrosurgical applications, the plasma action is primarily conducted by heating. Nevertheless, in the last fifteen years, attention has shifted towards the use of CAPs open to the air with temperatures below 40 °C [1,4], in order to explore other mechanisms of the action of plasma on cells and tissues that could be seized and exploited for therapeutic uses.

Plasma sources used in the development of therapeutic-type CAPs are of a very diverse type [4,6]. For each particular design, the experimental conditions of the discharge are optimized in order to generate the appropriate cocktail of reactive chemical species that, in their interaction with cells, tissues, or organs, give rise to certain desired therapeutic effects. Most CAPs use argon, helium, or air as the discharge support gas. In addition, they are usually open to the atmosphere, so they typically contain air to a greater or lesser extent, even when they have been generated in noble gases. They also have small amounts of water as a result of moisture in the air or the environment around them (tissues contain water). In fact, the presence of air and/or humidity in the plasma has been shown to be essential as it leads to the formation of ROS and RNS (reactive species containing oxygen and nitrogen, respectively), which play a key role in the therapeutic action of CAPs [15,16]. Thus, the characterization of these CAPs, including the identification and quantification of the active species generated in them, as well as the determination of their gas temperature are crucial issues that need to be addressed in order to understand the mechanisms triggered by their application to the human body. Of special relevance is the control of the gas temperature (T_g), which must always be kept below 40 °C to ensure

* Corresponding author.
E-mail address: fa1gamam@uco.es (M.C. García).

https://doi.org/10.1016/j.sab.2022.106437
Received 6 March 2022; Received in revised form 29 April 2022; Accepted 2 May 2022
Available online 7 May 2022

its action is not thermal. Knowing reliable gas temperature values is also important when it comes to model these cold plasma sources. Indeed, in recent years an important effort is also being made in the modeling of CAPs and their interaction with the human body in order to be able to understand their mechanisms of action [17–20].

The Rayleigh scattering method, determining the gas temperature through neutral density measurement, has been successfully used for the diagnosis of argon plasma jets [21]. Nevertheless, it is a non-adequate method for the diagnosis of helium jets open to the air because of the small Rayleigh cross-section of helium. Furthermore, this laser-based diagnostic is rather complex as it requires equipment relatively expensive which is not always available in the laboratory and needs to be applied with care in atmospheric plasma jets [21].

In general, UV-Optical Emission Spectroscopy (UV-OES) offers useful and easy-to-implement techniques for plasma diagnosis. The electron density and temperature, the excited species density, and the gas temperature of the plasma can be measured by UV-OES techniques. Regarding the measurement of gas temperature, methods based on the detection and analysis of rotational bands of diatomic species are highly standardized, both by tradition and because it is an easy-to-use technique, even by researchers whose field of research it is not close to emission spectroscopy. Indeed, the spectrometers necessary for the detection of these bands do not require high performance and are therefore cheap. In addition, available diatomic species band simulation programs such as LIFBASE, Specair, or MassiveOES (some of them for free) facilitate the determination of the rotational temperature from the measured spectra. Nevertheless, in non-equilibrium plasmas, rotational spectra not fitting a Boltzmann distribution are often found. Also, the equilibrium between rotational and translational degrees of freedom of the molecules in the plasma is not always achieved [22]. Therefore, the values of rotational temperature derived from these spectra should be interpreted carefully. As Bruggeman et al. show through detailed analysis, although the use of rotational bands for the determination of the gas temperature is quite widespread, it is not always justified [22].

In a previously published article, we presented a method to measure T_g in argon CAPs from two argon atomic lines, which enabled simultaneous determination of the amount of air present in the plasma as an impurity [23]. Now in this work, we propose a new tool to diagnose T_g in helium CAPs from the collisional broadening of certain helium atomic (He I) lines. Compared to argon plasmas, helium plasmas at atmospheric pressure have lower electron densities, higher electron temperatures, and more energetic metastable species. This leads to different chemistry in them and a different (chemical, clinical) action, which needs to be evaluated.

In contrast to methods based on the analysis of rotational spectra of diatomic species, gas temperature measurement ones relying on the analysis of line broadenings do not require the assumption of Boltzmann equilibrium in the plasma (which is not always met for all species). On the other hand, given that the use of CAPs via endoscopy inside the human body (where the environment is not air) is on the horizon, methods based on atomic lines take on special relevance [24]. The method proposed here has the additional advantage of allowing the simultaneous determination of the air concentration in the discharge, which is generally determined by other more complex chemical analysis techniques.

In the development of this new method, a careful analysis of the distinct mechanisms of broadening of different He I emission lines was necessary to know which of these lines are suitable for the determination of T_g and lead to reliable values of this plasma parameter. As it will be shown, this technique requires the use of higher resolution spectrometers than those needed for diatomic band analysis. However, small, high-sensitivity, high-resolution spectrometers have recently been commercialized at relatively low prices, enabling its use by non-specialists in the field of plasma spectroscopy (whose interest mainly focuses on the plasma application–clinical action). In this sense, this work aims to offer a clear guide to measure the gas temperature in helium CAPs that can be useful for all types of users. For this reason, and although some details of the method can be found elsewhere in previous works, we will review them here in a summarized way.

Finally, this technique was used to measure the air fraction and T_g of helium microwave-induced plasmas generated in different environments, and results were compared with rotational temperatures obtained from the simulation of the rovibrational band of some N_2 excited species present in the plasma.

2. Method

It is well known that the shape of the profiles and the broadening of the atomic lines emitted by a plasma are partly determined by certain properties of the plasma, such as the density and electronic temperature, the temperature of the gas, or its composition [25]. Based on this, and making a suitable choice, it is possible to measure these plasma properties from the detection of particular atomic lines [23,26–28]. Thus, for example, the Stark broadening of the H_β (Balmer series hydrogen atomic line) is a commonly used method to measure the electron density of plasmas [29].

The different mechanisms causing the broadening of the detected lines are described in detail in the references [23, 26, 30, 31], so now we will just review them briefly. Note here that the emitted lines cannot be registered as they actually are since they are altered by the detection system itself (spectrometer, detectors, …), which introduces the so-called *instrumental broadening*, mainly determined by the resolution of the spectrometer. The *natural broadening* of the lines is typically in the order of 0.00001 nm, much lower than the resolution of the available optical devices (at least, three orders of magnitude lower), so it can be neglected. The rest of the broadenings atomic lines experience are due to physical phenomena in the plasma itself, which for non-magnetized plasmas are: i) the Doppler effect due to the movement of the emitting atoms, and ii) and the collisions of the emitting atoms with surrounding particles (charged or not). Thereby, they are referred to as *Doppler broadening* and *collisional broadening*, respectively. Both instrumental and Doppler broadenings give rise to Gaussian-shaped profiles, while collisional broadenings lead to Lorentzian-shaped ones. As a result, the detected line can fit reasonably well to a Voigt profile with an FWHM $\Delta\lambda_V$, and from it, the FWHM corresponding to both the Gaussian ($\Delta\lambda_G$) and Lorentzian ($\Delta\lambda_L$) contributions can be obtained.

Let's focus on the analysis of collisional broadening, that is, the Lorentzian part of the profile. As already mentioned, this broadening results from the interaction of the emitting atom with particles of different nature, encompassing the so-called *Stark*, *van der Waals*, and *resonance* broadenings. The presence of charged particles around the emitting atom causes the *Stark broadening* of the emitted line. In non-thermal plasmas, where electrons are very fast compared to ions, electrons are primarily responsible for this broadening. In the case of helium atoms, this broadening gives rise to a Lorentzian profile whose FWHM $\Delta\lambda_S$ is determined by both electron temperature (T_e) and electron density (n_e) in the plasma:

$$\Delta\lambda_S \approx \omega_e(T_e)\frac{n_e}{10^{16}}\ (\mathrm{nm}) \tag{1}$$

where ω_e is the Stark parameter of the emission line (which has been calculated by Griem [25] and Konjevic [32,33]), and n_e is measured in cm^{-3}.

On the other hand, the *van der Waals broadening* comes from the interaction with neutral perturbers around the emitter, more specifically, from the dipole interaction of an excited atom with the induced dipole in a ground state atom or molecule. It originates Lorentzian-shaped line profiles with a FWHM $\Delta\lambda_W$ which is determined by the temperature of the emitters T_g (equals to the gas temperature of the plasma). It also depends on some line parameters (namely, the wavelength λ and the difference of squares of coordinate vectors of the upper

and lower level of the atomic transition $\langle \overline{R^2} \rangle = \langle \overline{R_U^2} \rangle - \langle \overline{R_L^2} \rangle$), the polarizability of perturbers interacting with the excited radiator α, the pressure P, and the atom-perturber reduced mass μ [30,34], all gathered in the so-called C_W constant:

$$\Delta\lambda_W = \frac{C_W}{T_g^{0.7}} \quad (nm) \tag{2}$$

$$C_W = \frac{8.18 \cdot 10^{-19} \lambda^2 \left(\alpha \langle \overline{R^2} \rangle\right)^{2/5} P}{k_B \mu^{3/10}} \tag{3}$$

where λ is given in nm, α in cm^3, μ in u, and $\langle \overline{R^2} \rangle$ in a_0 units. A detailed deduction of this expression can be found in reference [35].

For a non-pure helium plasma in which different types of disturbers might exist, Eq. (2) can be rewritten in terms of the molar fractions of the distinct perturbers ($\chi_{perturber,i}$) as follows

$$\Delta\lambda_W = \sum \chi_{perturber\ i} \frac{C_W^{perturber\ i}}{T_g^{0.7}} \quad (nm)$$
$$\sum_i \chi_{perturber\ i} = 1 \tag{4}$$

As CAPs usually contain some air because they are open to the atmosphere, for the sake of clarity, we will only consider χ_{He} and χ_{air}.

On the other hand, the *resonance broadening* also comes from the interaction of the emitter with neutral perturbers around it, in this case, ground-state atoms of the same element. It only affects lines from transitions whose upper or lower level have an electric dipole transition to the ground state (through a resonance line). A Lorentzian-shaped line profile results from resonance mechanism, with a FWHM $\Delta\lambda_R$ dependent on T_g as follows:

$$\Delta\lambda_R = \chi_{He} \frac{C_R}{T_g} \quad (nm) \tag{5}$$

where χ_{He} is the molar fraction of helium and C_R constant is given by [30,34]:

$$C_R \approx 8.6 \times 10^{-27} \left(\frac{g_i}{g_k}\right)^{1/2} \lambda^2 \lambda_r f_r \frac{P}{k_B} \tag{6}$$

In Eq. (6) λ is the wavelength of the observed line in nm; f_r and λ_r are the oscillator strength and wavelength in nm of the line; g_k and g_i are the statistical weights of its upper and lower levels, k_B the Boltzmann constant, and P is the pressure. The reader can find a detailed description on the way this equation is obtained in references [36, 37]. Note that Eq. (5) considers the possible presence of impurities in the helium plasma as it includes the molar fraction of helium.

In general, the collisional broadening of emission lines is determined by both Stark and van der Waals broadenings and might also have a resonance contribution. The idea now is to choose He I lines for which the van der Waals and resonance contributions are relatively large (with high C_W and C_R values) and for which, at the same time, the Stark broadening can be neglected in the range of temperatures and electron densities in which the CAPs operate. In this case, the $\Delta\lambda_L$ of the line will be only dependent on gas temperature and composition and given by:

$$\Delta\lambda_L = \Delta\lambda_{Coliss} = \underbrace{\chi_{He} \frac{C_W^{He}}{T_g^{0.7}} + \chi_{air} \frac{C_W^{air}}{T_g^{0.7}}}_{\Delta\lambda_W} + \underbrace{\chi_{He} \frac{C_R}{T_g}}_{\Delta\lambda_R} =$$
$$= (1 - \chi_{air}) \frac{C_W^{He}}{T_g^{0.7}} + \chi_{air} \frac{C_W^{air}}{T_g^{0.7}} + (1 - \chi_{air}) \frac{C_R}{T_g} \tag{7}$$

Because the fraction of air is unknown, the use of a pair of lines will provide an appropriate method to measure T_g and χ_{air}. The largest resonance broadenings affect lines with longest wavelengths, and at the same time, whose levels are connected to the ground state through resonance lines of great oscillator strength [34]. Among all resonance lines of atomic helium system, He I 58.43 nm has the highest oscillator strength [38]. Using the NIST Atomic Database [38], He I lines with levels connected to the ground state through He I 58.43 nm can be easily found, being He I 667.82 nm, He I 728.13 nm, and He I 886.37 nm those with the longest wavelength. Because He I 886.37 nm is a very weak line (usually difficult to detect), we have chosen the first two lines. In this way, using expressions in reference [34], with reduced masses $\mu_{He-He} = 2$ and $\mu_{He-air} \approx 3.51$, helium polarizability $\alpha_{He} = 2.05 \times 10^{-25}$ cm^3 [39], air polarizability $\alpha_{air} \approx 1.68 \times 10^{-24}$ cm^3 (calculated from O_2, N_2, and Ar polarizabilities [40]), and data from NIST Atomic Database we get the following expressions:

$$\Delta\lambda_L^{He\ I\ 667.82\ nm} = (1 - \chi_{air}) \frac{1.79}{T_g^{0.7}} + \chi_{air} \frac{3.51}{T_g^{0.7}} + (1 - \chi_{air}) \frac{26.24}{T_g} \quad (nm)$$
$$\Delta\lambda_L^{He\ I\ 728.13\ nm} = (1 - \chi_{air}) \frac{2.49}{T_g^{0.7}} + \chi_{air} \frac{4.87}{T_g^{0.7}} + (1 - \chi_{air}) \frac{31.20}{T_g} \quad (nm) \tag{8}$$

Fig. 1a-b illustrate the dependence of $\Delta\lambda_L$ on T_g and χ_{air} for He I 667.82 nm and He I 728.13 nm lines derived from (8), for a typical value of electron density $n_e = 5 \cdot 10^{13}$ cm^{-3}. It is worth noting the fact that $\Delta\lambda_L$ becomes progressively more sensitive to T_g variations as the gas temperature decreases, being the precision of this method particularly high between 300 and 400 K, which makes this approach especially suitable for the measurement of T_g in CAPs.

On the other hand, Fig. 2 (a)-(d) show the contribution of the Stark broadening to the $\Delta\lambda_L$ of He I 667.82 nm and He I 728.13 nm lines. Two very different gas compositions (0 and 80% of air) have been analyzed. From these results, it can be concluded that no matter the composition of the gas is for electron densities below $1 \cdot 10^{14}$ cm^{-3}, the contribution of the Stark effect to $\Delta\lambda_L$ can be neglected for the two chosen helium lines (which is even truer for T_g under 1000 K). The method would be then suitable for helium containing plasmas, provided that this electron density condition fulfills.

3. Measuring the gas temperature and the air fraction of helium atmospheric pressure plasmas with different environments

3.1. Experimental setup

Fig. 3 shows the experimental setup used for plasma generation. A surfatron device coupled the energy coming from a microwave (2.45 GHz) power supply to helium gas (gas flow rate ranging from 200 to 1500 sccm) within a quartz tube of 6–8 mm of inner and outer diameter, respectively, using relatively low microwave power (105 W). To get this, the usual electromagnetic field configuration created by the surfatron was altered by introducing in the discharge tube a small rectangular shaped Si (1,0,0) wafer (4 mm × 20 mm × 300 μm), in the way is shown in Fig. 4. Let's remark that sustenance of helium microwave-induced plasmas at atmospheric pressure in dielectric tubes is rather complex as it needs the injection of very high powers leading to gas temperatures high enough to cause tube melting, and usually requires complicated and expensive cooling systems [41]. The novel configuration proposed in this work circumvents this inconvenience.

Three different tubes were used (labelled as designs #1, #2, and #3, respectively) in order to modify the composition of the gas around the plasma (see Fig. 5). In design #1, the tube was fully open to the air at its end; in design #2, the tube has a narrower front end and an additional lateral opening. Finally, in design #3 the tube only has the lateral opening as schematized in Fig. 5. In the first case (design #1), flow rates explored ranged from 200 to 1500 sccm. On the other hand, in designs #2 and #3, the range of gas flow rate studied only varied from 200 and 600 sccm to avoid overpressure inside the tube, which could affect the collisional broadening of the lines.

Fig. 3 also includes a scheme of the optical detection assembly and data acquisition system to process OES measurements. A Czerny-Turner

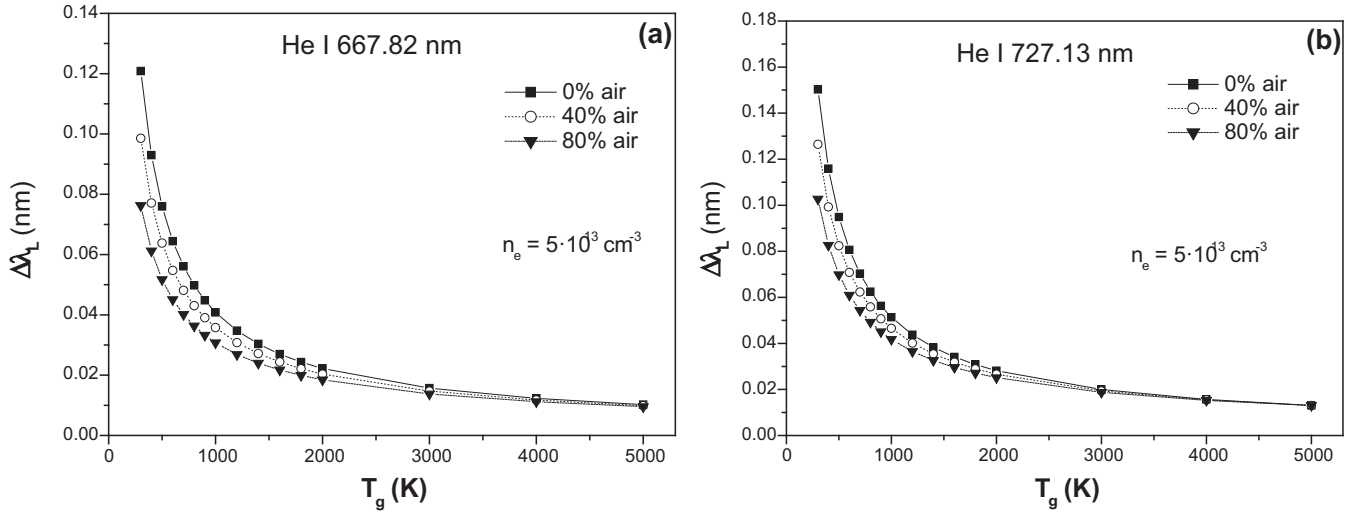

Fig. 1. Dependence of $\Delta\lambda_L$ on T_g and χ_{air} for (a) He I 667.82 nm and (b) He I 728.13 nm lines for a typical electron density $n_e = 5 \cdot 10^{13}$ cm^{-3}.

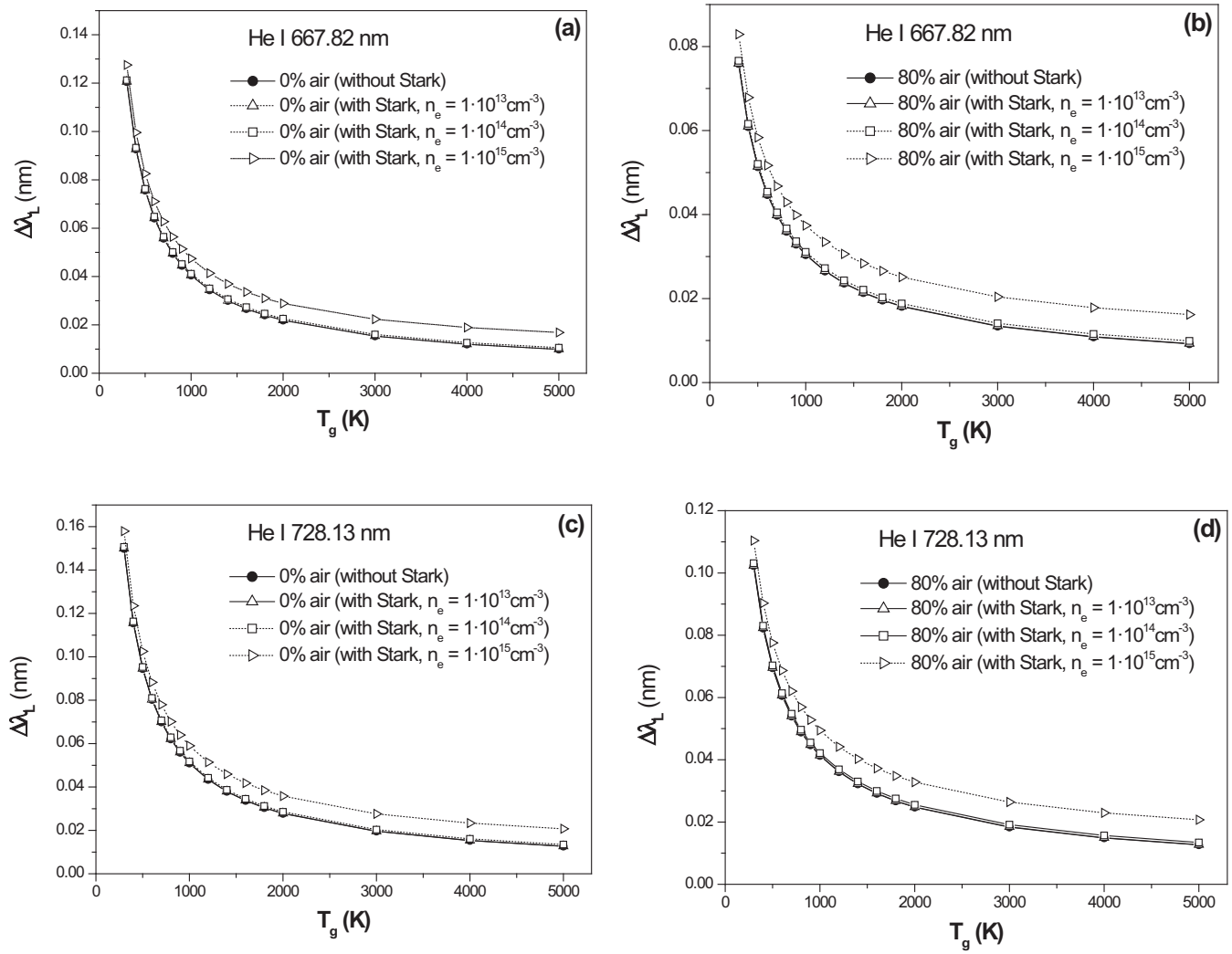

Fig. 2. Analysis of the contribution of the Stark broadening to the $\Delta\lambda_L$ of He I 667.82 nm and He I 728.13 nm lines for different conditions of electron density.

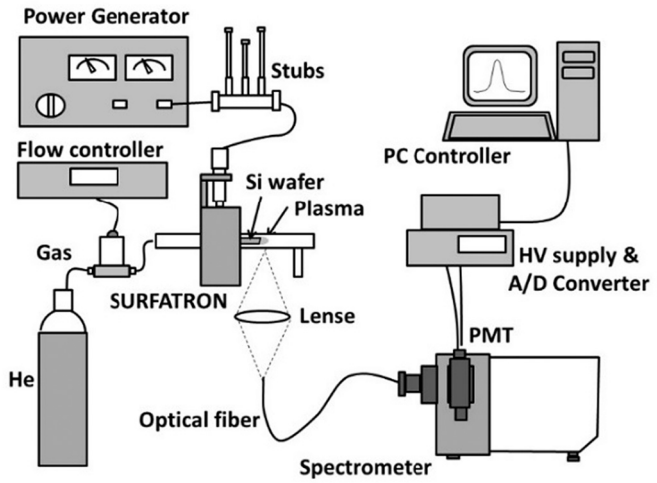

Fig. 3. Experimental setup.

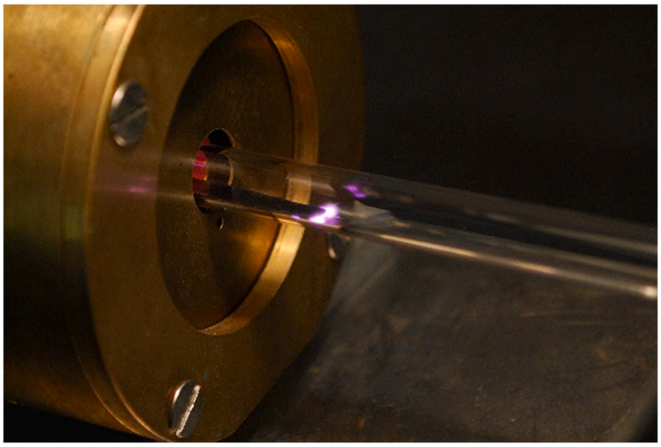

Fig. 4. Details of the MW helium plasma.

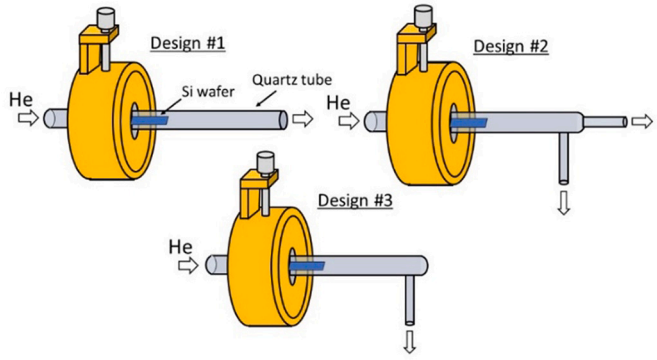

Fig. 5. Different tube designs used in this work.

type spectrometer of 1 m focal length (Jobin-Yvon THR1000), equipped with a 1200 grooves/mm holographic grating and an R636 Hamamatsu photomultiplier (PMT) as a detector, was used for the analysis of the plasma emission. The PMT was powered by a HV power supply (set at 1300 V) and the analogic signal from it was transformed into a digital one through an A/D converter (see Fig. 3). The recording of lines was performed using Jovin-Yvon software (Syner JY) with an integration time of 0.5 s. The emission was transversely collected from the most intense region of the plasma near the small silicon piece and focused onto an optical fiber using an achromatic lens.

We selected slits 37 μm width (which allowed the detection of relatively intense emission lines) for which the instrumental broadening corresponding to the wavelengths 667.82 and 728.13 nm took the values 0.0296 nm and 0.0292 nm, respectively [34]. Under these experimental conditions, the instrumental broadening of He I 667.82 and He I 728.13 nm lines mainly determined the Gaussian part of their respective profiles, as the Doppler broadening of these lines for 300 K $< T_g <$ 1000 K ranges from 0.004 to 0.008 nm.

The line H I 486.13 nm (H_β) was also recorded in order to measure plasma electron density following the procedure described in [29,42]. As already explained, knowledge of this plasma parameter enabled quantifying the Stark broadening of the lines and demonstrating that it was negligible under the experimental conditions of this helium atmospheric non-thermal plasma.

A commercial code (Peak-Fitting module, Microcal Origin©) was used to fit the atomic lines to a Voigt profile. In this way, both the area under the peak (scaling with the intensity of the line) and the $\Delta\lambda_V$ of the profile were obtained for each atomic line measured.

A self-absorption test was performed for the atomic lines detected, following the procedure described in reference [43]. Thus, profiles recorded with and without a mirror were compared. The line width did not change, which allowed concluding that none of the lines used in this work experienced self-absorption.

Finally, N_2 (C-B) rovibrational band (2nd positive system) at the region 370–381 nm was measured. MassiveOES code developed by Vorác et al. [44] was used for the determination of the gas temperature through the rotational temperature. In this way, T_g values obtained from both procedures could be compared.

In all cases, each spectrum was recorded six times and errors were determined from dispersion.

3.2. Results and discussion

Fig. 6 shows a typical UV-OES spectrum measured for this helium microwave-sustained plasma. It mainly consisted of excited nitrogen-containing species evidencing the presence the air in the discharge. Accordingly, atomic oxygen emission at 777 nm was also intense.

Table 1 shows the values of FWHM $\Delta\lambda_L$ measured for He I 667.82 and He I 728.13 nm lines in the different experimental conditions explored for the design #1 tube. The procedure followed to obtain them is that indicated by Rodero et al. in reference [34]. First, the lines were adjusted to a Voigt profile to find $\Delta\lambda_V^{exp}$ (see Fig. 7). Then, from it and the Gaussian FWHM $\Delta\lambda_G$ (encompassing instrumental and Doppler

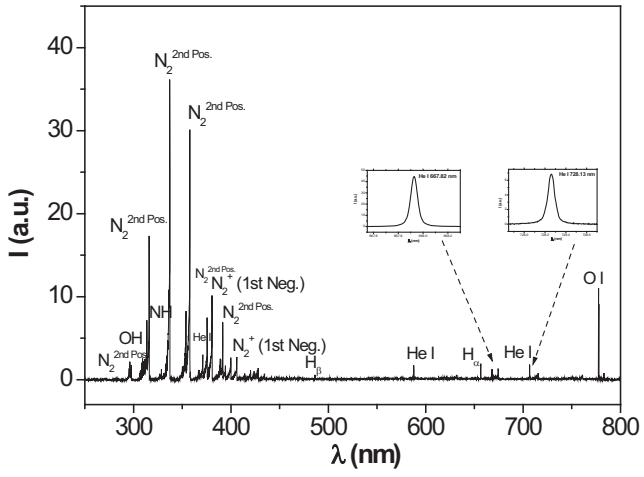

Fig. 6. Typical UV-OES spectrum measured for the helium microwave-sustained plasma.

Table 1
Experimental results for the helium plasma generated in design #1-tube.

F_{He} (sccm)	He I	$\Delta\lambda_V$ (nm)	$\Delta\lambda_L$ (nm)	$\Delta\lambda_G$ (nm)	T_g (K)	% Air	T_{rot} (K)
200	667.82 nm	0.0656 ± 0.0006	0.0517 ± 0.0007	0.0301	555 ± 10	65 ± 3	926
	728.13 nm	0.0796 ± 0.0005	0.0684 ± 0.0010	0.0298			
400	667.82 nm	0.0652 ± 0.0006	0.0512 ± 0.0007	0.0302	615 ± 11	50 ± 3	990
	728.13 nm	0.0782 ± 0.0005	0.0667 ± 0.0006	0.0299			
600	667.82 nm	0.0639 ± 0.0004	0.0496 ± 0.0005	0.0302	673 ± 8	40 ± 2	1010
	728.13 nm	0.0760 ± 0.0004	0.0642 ± 0.0004	0.0300			
900	667.82 nm	0.0635 ± 0.0003	0.0490 ± 0.0004	0.0303	733 ± 7	25 ± 2	980
	728.13 nm	0.0747 ± 0.0006	0.0626 ± 0.0006	0.0300			
1200	667.82 nm	0.0639 ± 0.0003	0.0496 ± 0.0004	0.0303	755 ± 6	15 ± 2	920
	728.13 nm	0.0750 ± 0.0002	0.0629 ± 0.0003	0.0300			
1500	667.82 nm	0.0632 ± 0.0002	0.0486 ± 0.0003	0.0304	810 ± 4	3 ± 2	975
	728.13 nm	0.0732 ± 0.0003	0.0612 ± 0.0002	0.0301			

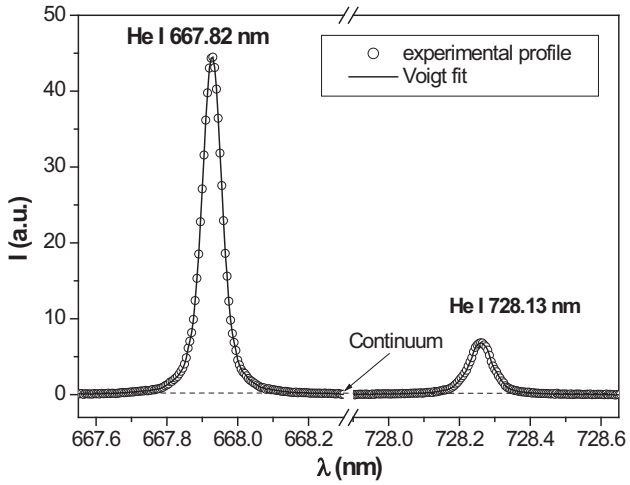

Fig. 7. Typical fitting of atomic lines to a Voigt profile (Design #2, F_{He} = 400 sccm).

broadenings), the Lorentzian part $\Delta\lambda_L$ was derived. Table 1 also includes the values of T_g and proportion of air resulting from these broadenings using expressions (8). In the same way, Tables 2 and 3 gather results corresponding to the plasmas generated in design #2 and #3 tubes, respectively.

Fig. 8 (a)-(d) gather the results obtained for the three different configurations investigated, including the gas temperature, the fraction of air, the intensity of the He I 667.82 nm line (measured from its area), and the electron density. The values of n_e were measured from the analysis of the collisional broadening of the H_β line following the procedure described in the references [26, 29, 42]. It is worth noting first, that values of n_e ranged from 2.3 to 6.0 × 10^{13} cm^{-3}. From them, and using Expression (1) with the Stark parameters for He I 667.82 and He I 728.13 nm lines given by Griem in [25] (0.0698 and 0.0806 nm, respectively, for T_e = 20,000 K), it was found that the Stark broadening of these lines was in the order of 0.0003 nm, in the range of experimental conditions explored in this work. Thus, it was once more verified that

Table 2
Experimental results for the helium plasma generated in design #2.

F_{He} (sccm)	He I	$\Delta\lambda_V$ (nm)	$\Delta\lambda_L$ (nm)	$\Delta\lambda_G$ (nm)	T_g (K)	% Air	T_{rot} (K)
200	667.82 nm	0.0637 ± 0.0002	0.0493 ± 0.0003	0.0301	618 ± 5	57 ± 1	1245 ± 50
	728.13 nm	0.0765 ± 0.0002	0.0645 ± 0.0002	0.0299			
400	667.82 nm	0.0631 ± 0.0005	0.0486 ± 0.0006	0.0302	683 ± 10	42 ± 3	1127 ± 65
	728.13 nm	0.0750 ± 0.0006	0.0630 ± 0.0004	0.0300			
600	667.82 nm	0.0629 ± 0.0005	0.0483 ± 0.0006	0.0303	715 ± 9	34 ± 3	1248 ± 70
	728.13 nm	0.0743 ± 0.0003	0.0622 ± 0.0004	0.0300			

Table 3
Experimental results for the helium plasma generated in design #3.

F_{He} (sccm)	He I	$\Delta\lambda_V$ (nm)	$\Delta\lambda_L$ (nm)	$\Delta\lambda_G$ (nm)	T_g (K)	% Air	T_{rot} (K)
200	667.82 nm	0.0637 ± 0.0004	0.0494 ± 0.0005	0.0302	625 ± 8	55 ± 2	1200 ± 40
	728.13 nm	0.0764 ± 0.0004	0.0647 ± 0.0005	0.0299			
400	667.82 nm	0.0634 ± 0.0002	0.0489 ± 0.0003	0.0304	815 ± 5	2 ± 2	1180 ± 65
	728.13 nm	0.0737 ± 0.0004	0.0614 ± 0.0004	0.0301			
600	667.82 nm	0.0626 ± 0.0005	0.0478 ± 0.0005	0.0304	835 ± 11	1 ± 1	1160 ± 45
	728.13 nm	0.0726 ± 0.0002	0.0601 ± 0.0002	0.0302			

the contribution of this broadening to the Lorentzian part of the profile of both lines (so, to the total collisional broadening) was indeed negligible, and the T_g determination method proposed in this work applied.

For the three configurations analyzed, progressively higher helium flow rates led to a decrease in the fraction of air. In design #1, the gas sustaining the discharge at F_{He} = 1500 sccm was mostly pure helium. In design #2 tube, the fraction of air detected was somewhat lower than in design #1 for F_{He} = 200, 400, and 600 sccm, which can be attributed to the fact that in this tube there was less air intake from the outside. For design #3, the fraction of air measured for F_{He} = 200 sccm was lower than in the two previous cases, and from F_{He} = 400 sccm this fraction was negligible, which indicates that this helium flow was capable of removing the majority of the air from the tube. Accordingly, for the three configurations, the intensity of the He I 667.82 nm line increased as the helium flow rate did, as a result of both the greater amount of helium and the progressively higher electron density leading to a better excitation. Finally, helium lines were more intense in designs #2 and #3 because of a greater accumulation of helium around the discharge for this tube configuration.

Tables 1–3 also gather the rotational temperature measured from simulations of N_2 (C-B) band at the region 370–381 nm using MassiveOES. As shown, the values of T_g *and* T_{rot} differ notably, especially in

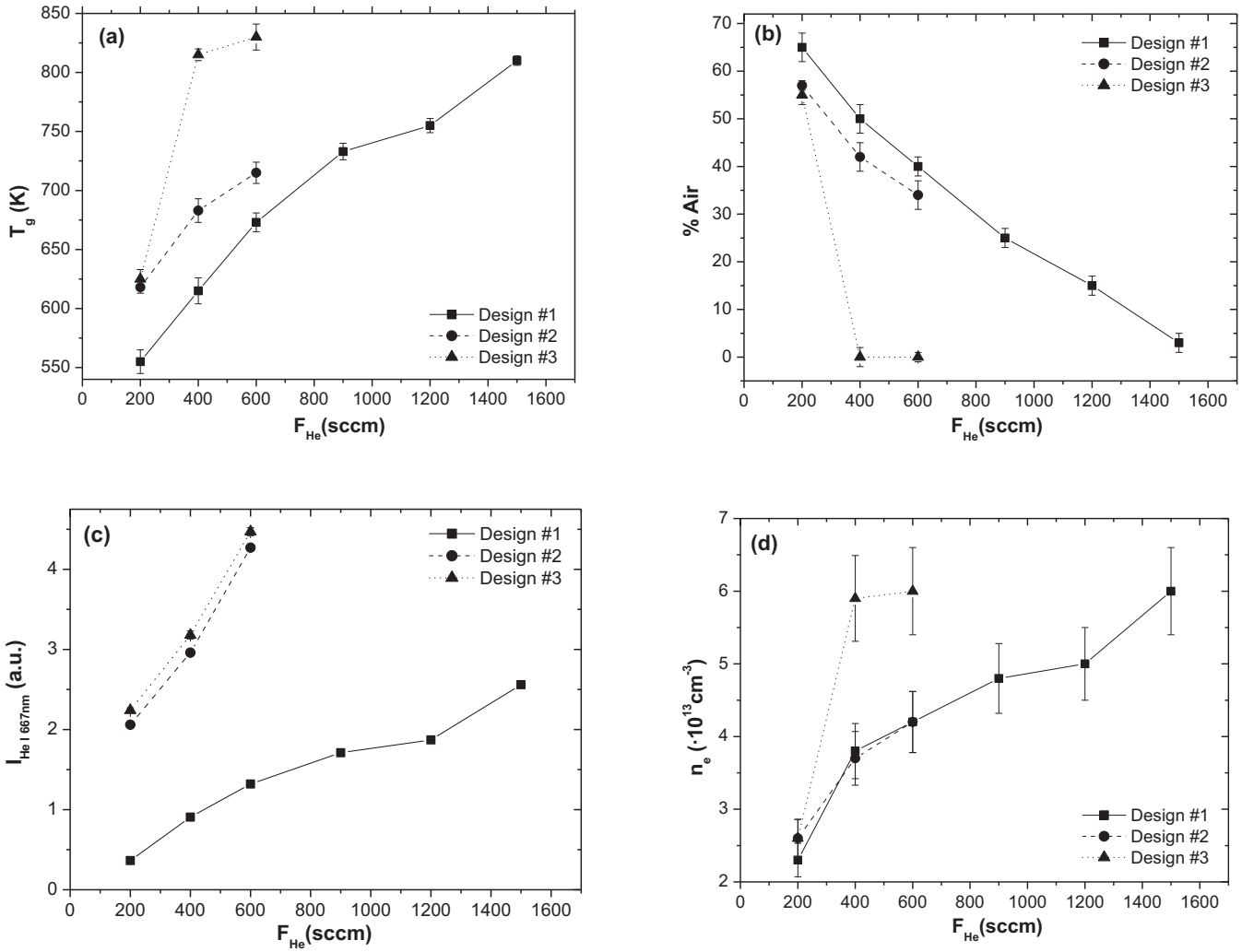

Fig. 8. Values of T_g, fraction of air, intensity of the He I 667.82 nm line, and n_e for the different helium plasmas explored in this work.

the cases with larger amounts of air. The unsuitability of T_{rot} values for gas temperature determination has been often reported. In non-equilibrium plasmas, some rotational states of certain diatomic species could not be in Boltzmann equilibrium. Neither is always achieved an equilibrium between rotational and translational degrees of freedom of the molecules. Bruggeman et al. [22] have performed a detailed and comprehensive analysis about the conditions under which the gas temperatures can be obtained from the spectra of some diatomic species. They claim that, in atmospheric pressure plasmas, the high collisionality is not a guarantee to achieve thermalized rotational distributions and recommend a careful analysis case by case (including an estimation of the effective lifetime of the excited state and its comparison with the rotational thermalization time) before assuming the rotational temperature can be considered equal to T_g. Here, we are not going to analyze the reasons of the disagreements we have confirmed as this falls out of the scope of the paper.

4. Final remarks

The measurement of the collisional broadening of the He I 667.82 nm and 728.13 nm lines allows the simultaneous determination of the gas temperature and the air fraction in non-thermal atmospheric helium plasmas, in general. Particularly noteworthy is the fact that this method, unlike rotational band analysis methods, is no-based on thermodynamic equilibrium assumptions. Moreover, this is a particularly accurate method under low gas temperature conditions ($<1000K$); hence it is especially suitable for the diagnosis of CAPs. For helium plasmas with electron densities below 10^{14} cm^{-3}, the contribution of the Stark broadening of these lines to the total collisional broadening can be neglected, which eases the determination of T_g (electron density in most helium CAPs is in the order of 10^{12}–10^{13} cm^{-3} [21,45–47]).

In applying this new method, it is necessary to know the resolution of the optical device at 667.82 nm and 728.13 nm, which determines the instrumental broadening of both helium lines. The smaller the instrumental broadening, the more accurate the method will be. However, since CAPs operate at low power, the intensity of these helium lines is often low, which requires wider spectrometer slits and results in a greater instrumental broadening. Nowadays, small, high-sensitivity, high-resolution spectrometers are already on the market at relatively low prices, making this technique affordable and more precise [48].

CRediT authorship contribution statement

M.C. García: Conceptualization, Methodology, Investigation, Formal analysis, Writing – original draft, Writing – review & editing, Visualization, Supervision. **C. Yubero:** Conceptualization, Methodology. **A. Rodero:** Conceptualization, Methodology, Investigation, Writing – review & editing, Supervision, Funding acquisition.

Declaration of Competing Interest

The authors declare that they have no known competing financial interests or personal relationships that could have appeared to influence the work reported in this paper.

Ackowledgments

Authors thank the FEDER program and the Spanish Ministry of Science and Innovation (PID2020-112620GB-I00 and PID2020-114270RA-I00 Grants, MCIN/AEI/10.13039/501100011033). They are also indebted to the *Física de Plasmas: Diagnosis, Modelos y Aplicaciones (FQM 136)* research group of Regional Government of Andalusia for Technical and Financial Support.

References

[1] M. Laroussi, Cold plasma in medicine and healthcare: the new frontier in low temperature plasma applications, Front. Phys. 8 (2020) 1–7, https://doi.org/10.3389/fphy.2020.00074.
[2] S. Bekeschus, P. Favia, E. Robert, T. von Woedtke, White paper on plasma for medicine and hygiene: future in plasma health sciences, Plasma Process. Polym. 16 (2019), e1800033, https://doi.org/10.1002/ppap.201800033.
[3] R. Brandenburg, A. Bogaerts, W. Bonger, A. Fridman, G. Fridman, B.R. Locke, V. Miller, S. Reuter, M. Schiorlin, T. Verreycken, K. Ostrikov, White paper on the future of plasma science in environment, for gas conversion and agriculture, Plasma Process. Polym. 16 (2019), e1700238, https://doi.org/10.1002/ppap.201700238.
[4] T. von Woedtke, S. Reuter, K. Masur, K.D. Weltmann, Plasmas for medicine, Phys. Rep. 530 (2013) 291–320, https://doi.org/10.1016/j.physrep.2013.05.005.
[5] S. Bekeschus, A. Schmidt, K.D. Weltmann, T. von Woedtke, The plasma jet kINPen-A powerful tool for wound healing, Clin. Plasma Med. 4 (2016) 19–28, https://doi.org/10.1016/j.cpme.2016.01.001.
[6] J. Gay-Mimbrera, M.C. García, B. Isla-Tejera, A. Rodero-Serrano, A. Vélez-Nieto, J. Ruano, Clinical and biological principles of cold atmospheric plasma application in skin cancer, Ad. Ther. 33 (2016) 894–909, https://doi.org/10.1007/s12325-016-0338-1.
[7] H.R. Metelmann, C. Seebauer, V. Miller, A. Fridman, G. Bauer, D.B. Graves, J. M. Pouvesle, R. Rutkowski, M. Schuster, S. Bekeschus, K. Wende, K. Masur, S. Hasse, T. Gerling, M. Hori, H. Tanaka, E.H. Choi, K.D. Weltmann, P. H. Metelmann, D.D. Von Hoff, T. von Woedtke, Clinical experience with cold plasma in the treatment of locally advanced head and neck cancer, Clin. Plasma Med. 9 (2018) 6–13, https://doi.org/10.1016/j.cpme.2017.09.001.
[8] T. Bernhardt, M.L. Semmler, M. Schäfer, S. Bekeschus, S. Emmert, L. Boeckmann, Plasma medicine: applications of cold atmospheric pressure plasma in dermatology, Oxidative Med. Cell. Longev. (2019), https://doi.org/10.1155/2019/3873928. Article ID 3873928.
[9] K.E. Grund, D. Storek, G. Farin, Endoscopic argon plasma coagulation (APC): first clinical experiences in flexible endoscopy, Endosc. Surg. Allied. Technol. 2 (1994) 42–46.
[10] T. Sagawa, T. Takayama, T. Oku, T. Hayashi, H. Ota, T. Okamoto, H. Muramatsu, S. Katsuki, Y. Sato, J. Kato, Y. Niitsu, Argon plasma coagulation for successful treatment of early gastric cancer with intramucosal invasion, Gut 52 (2003) 334–339, https://doi.org/10.1136/gut.52.3.334.
[11] J. Raiser, M. Zenker, Argon plasma coagulation for open surgical and endoscopic applications: state of the art, J. Phys. D. Appl. Phys. 39 (2006) 3520–3523, https://doi.org/10.1088/0022-3727/39/16/S10.
[12] http://medicaldevices.com.ar/coblation/ (last access: 03/01/2022).
[13] M. Omrani, B. Barati, N. Omidifar, A.R. Okhovvat, S.A.G. Hashemi, Coblation versus traditional tonsillectomy: a double blind randomized controlled trial, J. Res. Med. Sci. 17 (2012) 45–50.
[14] T.K. Madhuri, D. Papatheodorou, A. Tailor, C. Sutton, S. Butler-Manuel, First clinical experience of argon neutral plasma energy in gynaecological surgery in the UK, Gynecol. Surg. 7 (2010) 423–425, https://doi.org/10.1007/s10397-010-0591-2.
[15] D.B. Graves, The emerging role of reactive oxygen and nitrogen species in redox biology and some implications for plasma applications to medicine and biology, J. Phys. D. Appl. Phys. 45 (2012) 263001 (42pp), https://doi.org/10.1088/0022-3727/45/26/263001.
[16] X. Dai, K. Bazaka, E.W. Thompson, K. Ostrikov, Cold atmospheric plasma: a promising controller of cancer cell states, Cancers 12 (2020) 3360, https://doi.org/10.3390/cancers12113360.
[17] S.A. Norberg, W. Tian, E. Johnsen, M.J. Kushner, Atmospheric pressure plasma jets interacting with liquid covered tissue: touching and not-touching the liquid, J. Phys. D. Appl. Phys. 47 (2014) 475203 (11pp), https://doi.org/10.1088/0022-3727/47/47/475203.
[18] W. Tian, M.J. Kushner, Atmospheric pressure dielectric barrier discharges interacting with liquid covered tissue, J. Phys. D. Appl. Phys. 47 (2014) 165201 (21pp), https://doi.org/10.1088/0022-3727/47/16/165201.
[19] A.M. Lietz, M.J. Kushner, Electrode configurations in atmospheric pressure plasma jets: production of reactive species, Plasma Sources Sci. Technol. 27 (2018) 105020 (26pp), https://doi.org/10.1088/1361-6595/aadf5b.
[20] H.W. Lee, G.Y. Park, Y.S. Seo, Y.H. Im, S.B. Shim, H.J. Lee, Modelling of atmospheric pressure plasmas for biomedical applications, J. Phys. D. Appl. Phys. 44 (2011), 053001 (27pp), https://doi.org/10.1088/0022-3727/44/5/053001.
[21] S. Hofmann, A.F.H. van Gessel, T. Verreycken, P. Bruggeman, Power dissipation, gas temperatures and electron densities of cold atmospheric pressure helium and argon RF plasma jets, Plasma Sources Sci. Technol. 20 (2011), 065010 (12pp), https://doi.org/10.1088/0963-0252/20/6/065010.
[22] P.J. Bruggeman, N. Sadeghi, D.C. Schram, V. Linss, Gas temperature determination from rotational lines in non-equilibrium plasmas: a review, Plasma Sources Sci. Technol. 23 (2014), 023001 (32pp), https://doi.org/10.1088/0963-0252/23/2/023001.
[23] M.C. Garcia, C. Yubero, A. Rodero, Measuring the air fraction and the gas temperature in non-thermal argon plasma jets through the study of the air influence on the collisional broadening of some argon atomic emission lines, Plasma Sources Sci. Technol. 29 (2020), 055006 (7pp), https://doi.org/10.1088/1361-6595/ab87b8.
[24] B. Hillebrand, E. Iglesias, A.R. Gibson, N. Bibinov, A. Neugebauer, M. Enderle, P. Awakowicz, Determination of plasma parameters by spectral line broadening in an electrosurgical argon plasma, Plasma Sources Sci. Technol. 29 (2021) 125011, https://doi.org/10.1088/1361-6595/abc411.
[25] H.R. Griem, Spectral Line Broadening by Plasmas, Academic, New York, 1974.
[26] C. Yubero, M.D. Calzada, M.C. Garcia, Using the stark broadening of the Halpha, Hbeta and Hgamma lines for the measurement of Electron density and temperature in a plasma at atmospheric pressure, J. Phys. Soc. Jpn. 74 (2005) 2249–2254, https://doi.org/10.1143/JPSJ.74.2249.
[27] C. Yubero, M.C. Garcia, M. Varo, P. Martinez, Gas temperature determination in microwave discharges at atmospheric pressure by using different optical emission spectroscopy techniques, Spectrochim. Acta B 90 (2013) 61–67, https://doi.org/10.1016/j.sab.2013.10.004.
[28] C. Yubero, A. Rodero, M. Dimitrijevic, A. Gamero, M.C. Garcia, Gas temperature determination in a non-thermal plasma at atmospheric pressure from broadenings of atomic emission lines, Spectrochim. Acta B 129 (2017) 14–20, https://doi.org/10.1016/j.sab.2017.01.002.
[29] A.Y. Nikiforov, C. Leys, M.A. Gonzalez, J.L. Walsh, Electron density measurement in atmospheric pressure plasma jets: stark broadening of hydrogenated and non-hydrogenated lines, Plasma Sources Sci. Technol. 24 (2015), 034001 (18pp), https://doi.org/10.1088/0963-0252/24/3/034001.
[30] W.C. Martin, W.L. Wiese, Chapter 10 in Springer Handbook of Atomic, Molecular, and Optical Physics (G. Drake Ed.), Springer, New York, 2006.
[31] N. Konjevic, Plasma broadening and shifting of non-hydrogenic spectral lines: present status and applications, Phys. Rep. 316 (1999) 339–401, https://doi.org/10.1016/S0370-1573(98)00132-X.
[32] N. Konjevic, W.L. Wiese, Experimental stark widths and shifts for spectral lines of neutral and ionized atoms, J. Phys. Chem. Ref. Data 19 (1990) 1307–1990, https://doi.org/10.1063/1.555847.
[33] N. Konjevic, A. Lesage, J.R. Fuhr, W.L. Wiese, Experimental stark widths and shifts for spectral lines of neutral and ionized atoms (a critical review of selected data for the period 1989 through 2000), J. Phys. Chem. Ref. Data 31 (2002) 819–927, https://doi.org/10.1063/1.1486456.
[34] A. Rodero, M.C. Garcia, Gas temperature determination of non-thermal atmospheric plasmas from the collisional broadening of argon atomic emission lines, J. Quant. Spectrosc. Radiat. Transf. 198 (2017) 93–103, https://doi.org/10.1016/j.jqsrt.2017.05.004.
[35] C. Yubero, M.S. Dimitrijevic, M.C. Garcia, M.D. Calzada, Using the van der Waals broadening of the spectral atomic lines to measure the gas temperature of an argon microwave plasma at atmospheric pressure, Spectrochim. Acta B 62 (2007) 169–176, https://doi.org/10.1016/j.sab.2007.02.008.
[36] A.W. Ali, H.R. Griem, Theory of resonance broadening of spectral lines by atom-atom impacts, Phys. Rev. 140 (1965) 1044–1049.
[37] A.W. Ali, H.R. Griem, Theory of resonance broadening of spectral lines by atom-atom impacts (ERRATA), Phys. Rev. 144 (1966) 366.
[38] A. Kramida, Y. Ralchenko, J. Reader, NIST ASD Team, NIST Atomic Spectra Database (version 5.9), [Online], Available, https://physics.nist.gov/asd [Wed Dec 15 2021], National Institute of Standards and Technology, Gaithersburg, MD, , https://doi.org/10.18434/T4W30F.
[39] P. Schwerdtfegera, J.K. Nagle, Table of static dipole polarizabilities of the neutral elements in the periodic table\mathrel{\raise1pt *\raise0pt}, Mol. Phys. 117 (2019) (2018) 1200–1225, https://doi.org/10.1080/00268976.2018.1535143.
[40] https://cccbdb.nist.gov/xp1x.asp?prop=9 (last access: 03/02/2022).
[41] J. Muñoz, J. Margot, M.D. Calzada, Experimental study of a helium surface-wave discharge at atmospheric pressure, J. Appl. Phys. 107 (2010), 083304, https://doi.org/10.1063/1.3346122.
[42] Y.E. Kovach, M.C. García, J.E. Foster, Optical emission spectroscopy investigation of a 1-atm DC glow discharge with liquid anode and associated self-organization patterns, IEEE Trans. Plasma Sci. 47 (2019) 3214–3227, https://doi.org/10.1109/TPS.2019.2918065.
[43] S.S. Ivkovic, G.B. Sretenovic, B.M. Obradovic, N. Cvetanovic, M.M. Kuraica, On the use of the intensity ratio of He lines for electric field measurements in atmospheric pressure dielectric barrier discharge, J. Phys. D. Appl. Phys. 47 (2014) 055204 (10pp) 4 (10pp), https://doi.org/10.1088/0022-3727/47/5/055204.
[44] J. Vorác, P. Synek, L. Potocnáková, J. Hnilica, V. Kudrle, Batch processing of overlapping molecular spectra as a tool for spatio-temporal diagnostics of power

modulated microwave plasma jet, Plasma Sources Sci. Technol. 2 (2017), 025010, https://doi.org/10.1088/1361-6595/aa51f0.

[45] G.V. Naidis, Modelling of plasma bullet propagation along a helium jet in ambient air, J. Phys. D. Appl. Phys. 44 (2011) 215203 (5pp), https://doi.org/10.1088/0022-3727/44/21/215203.

[46] J.P. Boeuf, L.L. Yang, L.C. Pitchford, Dynamics of a guided streamer ('plasma bullet') in a helium jet in air at atmospheric pressure, J. Phys. D. Appl. Phys. 46 (2013), 015201 (13pp). (13pp), https://doi.org/10.1088/0022-3727/46/1/015201.

[47] A.M. Lietz, E.V. Barnat, J.E. Foster, M.J. Kushner, Ionization wave propagation in a He plasma jet in a controlled gas environment, J. Appl. Phys. 128 (2020), 083301, https://doi.org/10.1063/5.0020264.

[48] F. Labelle, A.J. Durocher, L. Stafford, On the rotational-translational equilibrium in non-thermal argon plasmas at atmospheric pressure, Plasma Sources Sci. Technol. 30 (2021), 035020, https://doi.org/10.1088/1361-6595/abe91d.